CYP26A1 and CYP26C1 cooperatively regulate anterior–posterior patterning of the developing brain and the production of migratory cranial neural crest cells in the mouse

Masayuki Uehara [a], Kenta Yashiro [a,*], Satoru Mamiya [a], Jinsuke Nishino [a,1], Pierre Chambon [b], Pascal Dolle [b], Yasuo Sakai [a,2]

[a] *Developmental Genetics Group, Graduate School of Frontier Biosciences, Osaka University, and CREST, Japan Science and Technology Corporation (JST), 1-3 Yamada-oka, Suita, Osaka 565-0871, Japan*
[b] *Institut de Genetique et de Biologie Moleculaire et Cellulaire, CNRS/INSERM/ULP/College de France, BP10142, 67404 Illkirch Cedex, C.U. de Strasbourg, France*

Abstract

The appropriate regulation of retinoic acid signaling is indispensable for patterning of the vertebrate central nervous system along the anteroposterior (A–P) axis. Although both CYP26A1 and CYP26C1, retinoic acid-degrading enzymes that are expressed at the anterior end of the gastrulating mouse embryo, have been thought to play an important role in central nervous system patterning, the detailed mechanism of their contribution has remained largely unknown. We have now analyzed CYP26A1 and CYP26C1 function by generating knockout mice. Loss of CYP26C1 did not appear to affect embryonic development, suggesting that CYP26A1 and CYP26C1 are functionally redundant. In contrast, mice lacking both CYP26A1 and CYP26C1 were found to manifest a pronounced anterior truncation of the brain associated with A–P patterning defects that reflect expansion of posterior identity at the expense of anterior identity. Furthermore, $Cyp26a1^{-/-}Cyp26c1^{-/-}$ mice fail to produce migratory cranial neural crest cells in the forebrain and midbrain. These observations, together with a reevaluation of $Cyp26a1$ mutant mice, suggest that the activity of CYP26A1 and CYP26C1 is required for correct A–P patterning and production of migratory cranial neural crest cells in the developing mammalian brain.
© 2006 Published by Elsevier Inc.

Keywords: Central nervous system; CYP26; Anteroposterior axis; Neural crest cells; Retinoic acid

Introduction

Retinoic acid (RA) plays important roles in vertebrate embryonic development. Vitamin A deficiency (VAD) results in a spectrum of developmental malformations known as VAD syndrome (Thompson et al., 1969; Wilson et al., 1953), whereas intake of excess RA during pregnancy induces malformations referred to as RA embryopathy (Lammer et al., 1985; Ross et al., 2000). Animal models of VAD syndrome and RA embryopathy suggest that RA is especially important for development of the central nervous system (CNS). For instance, treatment of chick or mouse embryos with an excess of RA results in the loss of anterior structures including the forebrain, most of the midbrain, and eyes, whereas the hindbrain and spinal cord appear to expand in compensation (Maden, 2002). Such effects have been observed in various vertebrates when RA is administered at primitive streak stages (Avantaggiato et al., 1996; Simeone et al., 1995). The absence of signaling by RA receptors has also been shown to be required for rostral head formation (Koide et al., 2001). On the other hand, an imposed

reduction in the extent of RA signaling in developing embryos results in sequential loss of the posterior hindbrain (Dupe and Lumsden, 2001; Maden, 2002; Maden et al., 1996; Niederreither et al., 2000). These observations thus indicate that RA acts as a posteriorizing factor in patterning of the CNS along the anterior–posterior (A–P) axis.

The intracellular level of active RA is determined by the balance between its synthesis by retinaldehyde dehydrogenases (RALDHs) and its degradation by CYP26 enzymes, the latter of which constitute a group of P450 enzymes that metabolize RA to inactive forms (Fujii et al., 1997; Ray et al., 1997; White et al., 1996). CYP26 enzymes are thought to play a central role in appropriate regulation of the RA signal as a posteriorizing factor in CNS development (Abu-Abed et al., 2001; Sakai et al., 2001; Sirbu et al., 2005). Mice and humans possess three CYP26 genes: *Cyp26a1*, *Cyp26b1*, and *Cyp26c1* (MacLean et al., 2001; Nebert and Russell, 2002; Tahayato et al., 2003).

During development of the early mouse embryo, RALDH2 is expressed in the paraxial mesoderm, somites, and lateral plate and serves as a source of RA (Niederreither et al., 1999). Among the three *Cyp26* genes, *Cyp26a1* is initially expressed in the head mesenchyme and neuroectoderm of mouse embryos at embryonic day (E) 7.5, whereas *Cyp26c1* is expressed only in the head mesenchyme at the same time (see Fig. 1A). In contrast, *Cyp26b1* expression begins in the prospective hindbrain at E8.0 (MacLean et al., 2001). *Cyp26a1* mutant mice manifest abnormal patterning of the hindbrain (Abu-Abed et al., 2001; Sakai et al., 2001), although this phenotype is not as severe as that expected from the pharmacological studies with RA. Moreover, no obvious malformation was observed in the CNS of *Cyp26b1* mutant mice (Yashiro et al., 2004). Although these studies have implicated CYP26 enzymes in regulation of RA signaling during CNS patterning, the expression of the other *Cyp26* genes in the *Cyb26a1* or
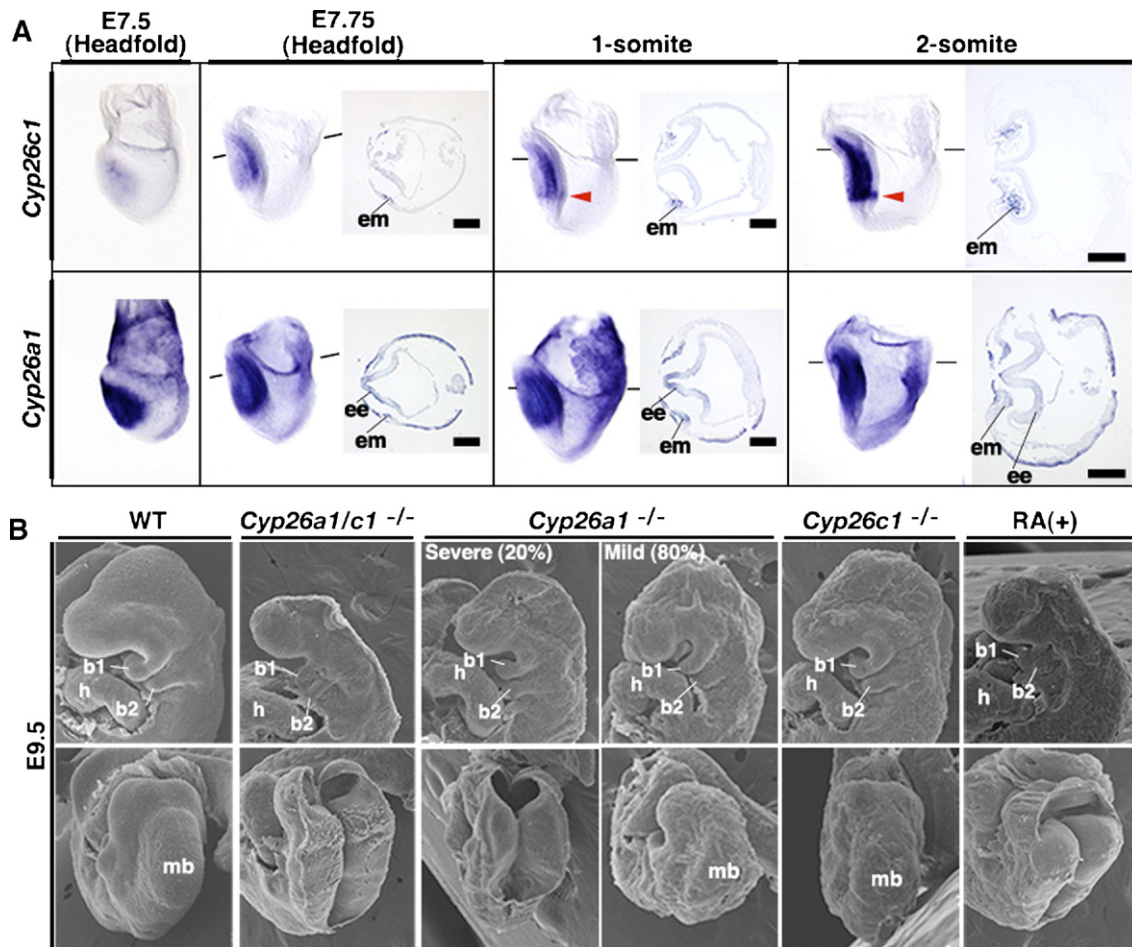

Fig. 1. CNS abnormalities in *Cyp26a1/c1$^{-/-}$* embryos. (A) Comparison of the patterns of *Cyp26c1* and *Cyp26a1* expression from the headfold to two-somite stages of wild-type (WT) mouse embryos as revealed by whole-mount in situ hybridization. During the period examined, *Cyp26c1* and *Cyp26a1* are expressed in the mesoderm of the anterior region, whereas *Cyp26a1* is also expressed in the neural plate and in the extraembryonic endoderm. The planes of sectioning are indicated by the lines through the corresponding embryos. Red arrowheads indicate *Cyp26c1* expression in r4. ee, embryonic ectoderm; em, embryonic mesoderm. Scale bars, 100 μm. (B) Scanning electron micrographs of WT, *Cyp26a1$^{-/-}$*, *Cyp26c1$^{-/-}$*, *Cyp26a1/c1$^{-/-}$*, and RA-treated [(RA(+)] WT embryos at E9.5. Lateral (upper panels) and dorsal (lower panels) views are shown for each embryo. Whereas *Cyp26c1$^{-/-}$* embryos appeared normal, *Cyp26a1/c1$^{-/-}$* embryos manifested pronounced CNS abnormalities, including an underdeveloped head and an open neural tube between the forebrain and hindbrain; the neural tube in the trunk region was closed (data not shown). Two representative *Cyp26a1$^{-/-}$* embryos are shown, one with an open neural tube (left) and the other with no obvious CNS defects (right). WT embryos exposed to exogenous RA at both E7.5 and E8.5 developed CNS defects similar to those of *Cyp26a1/c1$^{-/-}$* embryos. b1, first branchial arch; b2, second branchial arch; h, heart; mb, midbrain.

Cyp26b1 mutant mice may have masked a role for these latter genes in this process. A recent study suggested that CYP26C1 performs a function distinct from that of CYP26A1 in CNS patterning along the A–P axis (Sirbu et al., 2005), but the detailed contributions of these enzymes have remained unclear, mostly because of the lack of information on the effects of loss of CYP26C1 function in mice.

We have now generated mice that lack either *Cyp26c1* alone or both *Cyp26c1* and *Cyp26a1* in order to provide insight into the physiological functions of CYP26 enzymes in CNS development. Our data suggest that a differential distribution of RA generated by CYP26A1 and CYP26C1 patterns the developing brain along the A–P axis and regulates organ development from cranial neural crest cells (NCCs).

Materials and methods

Generation of Cyp26c1⁻/⁻ mice

The targeting vector contained a loxP-FRT-neo-FRT cassette inserted into intron 5 and a loxP cassette inserted into the 3′ untranslated region of *Cyp26c1* (Supplementary Fig. 1). Six embryonic stem (ES) cell clones were confirmed to have undergone homologous recombination. Two such clones (D10, K7) were subjected to electroporation in the presence of an expression vector for Cre recombinase, resulting in the generation of an allele that lacks exon 6 (*Cyp26c1⁻*). Two resulting clones (D10′, K7′) were used to generate *Cyp26c1⁻/⁻* mice in the present study.

Generation of Cyp26a1/c1⁻/⁻ mice

The targeting vector contained a 19-kb region encompassing *Cyp26c1* as well as a loxP-FRT-neo-FRT cassette inserted at the *Xba*I site in the 5′ region of the gene (Supplementary Fig. 2). The linearized targeting vector was introduced into an ES cell line (R19–R93) in which one of the *Cyp26a1* alleles had already been deleted (Sakai et al., 2001). ES clones in which the neo cassette was incorporated into the chromosome containing the *Cyp26a1⁻* allele were obtained. Two such ES clones (C5, G15) were subjected to electroporation in the presence of a Cre expression vector, resulting in the generation of a chromosome lacking both *Cyp26a1* and *Cyp26c1* (*Cyp26a1/c1⁻*). Two resulting clones (C5′, G15′) were used to generate *Cyp26a1/c1⁺/⁻* mice (B6/129 mixed background).

RA treatment

RA treatment was performed as previously described (Yashiro et al., 2004) with minor modifications. Pregnant ICR females were thus administered all-*trans*-RA (8 mg kg⁻¹, Sigma) in sesame oil (Sigma) by oral gavage. Control females received sesame oil only.

Histological analysis

In situ hybridization was performed with whole-mount preparations as previously described (Sakai et al., 2001). The RA signal was detected in embryos as previously described (Sakai et al., 2001) after crossing *Cyp26a1/c1⁺/⁻* mice harboring the *RARE-hsplacZ* transgene (Rossant et al., 1991) with *Cyp26a1/c1⁺/⁻* mice. The resulting embryos were subjected to genotyping and staining with 5-bromo-4-chloro-3-indolyl-β-D-galactopyranoside (X-gal, Wako) or 6-chloro-3-indolyl-β-D-galactopyranoside (Rose-gal, Slater and Frith).

Antibodies

Immunohistochemical analysis was performed with primary antibodies specific for E-cadherin (uvomorulin) (1:90 dilution, Sigma), N-cadherin (1:100 dilution, Zymed), mature caspase-3 (1:200 dilution, Cell Signaling Technology), or phosphorylated histone H3 (Upstate Biotechnology). Immune complexes were detected with Alexa568- or Alexa488-conjugated secondary antibodies to rabbit or mouse immunoglobulin G (1:400 dilution, Molecular Probes) or with a peroxidase-based Vectastain kit (Vector). Neurofilament staining with a monoclonal antibody (2H3; Developmental Studies Hybridoma Bank, Iowa University) was performed for whole-mount detection of cranial nerves as previously described (Sakai et al., 2001).

Analysis of the fates of cranial NCCs

Microinjection of DiI (1,1-dioctadecyl-3,3,3′,3′-tetramethylindocarbocyanine perchlorate, Molecular Probes) was performed as previously described (Inoue et al., 2000). Mouse embryos that developed to the zero- to two-somite stage were selected for DiI labeling. To label premigratory NCCs, we focally injected DiI into the presumptive midbrain and rhombomere 4 (r4) regions. The embryos were then cultured for 24 h as previously described (Nonaka et al., 2002) before fixation with 4% paraformaldehyde in phosphate-buffered saline and examination with a Leica MZ FL III stereomicroscope.

Results

Cyp26c1⁻/⁻ mice exhibit normal CNS development

First, to examine the role of *Cyp26c1* in embryogenesis, we generated *Cyp26c1* knockout mice (Supplementary Fig. 1). However, these animals did not manifest overt anatomic abnormalities (Fig. 1B, data not shown). Although CYP26C1 was previously suggested to restrict the anterior border of the RA signal in the CNS to the boundary between r4 and r5 after E8.0 (Sirbu et al., 2005), this border was intact in the *Cyp26c1* null mutant (Supplementary Fig. 3). Our results thus indicate that CYP26C1 alone is not required for CNS development and formation of the anterior border of the RA signal at r4–r5.

Cyp26c1 is chromosomally linked with *Cyp26a1*, and the two genes are expressed in overlapping domains (Tahayato et al., 2003). The lack of apparent defects in *Cyp26c1* knockout mice might therefore be due to functional redundancy between *Cyp26c1* and *Cyp26a1*. Consistent with this notion, *Cyp26a1* expression is maintained within the normal range in *Cyp26c1⁻/⁻* embryos (Supplementary Fig. 4A). Most *Cyp26a1* null embryos show a mild hindbrain anomaly, in contrast to the marked abnormalities of RA-treated animals (Fig. 1B) (Maden, 2002), suggesting that the effects of exogenous RA are nonphysiological or that CYP26C1 may play a role in CNS patterning in cooperation with CYP26A1. To examine the functional relation between these two enzymes, we examined the expression patterns of both genes in wild-type (WT) embryos from the headfold to two-somite stages (Fig. 1A). The two genes showed similar expression patterns at each stage, although some differences were observed (Sirbu et al., 2005). The expression of both genes begins in the mesenchyme of the anterior region at the headfold stage, although the expression level of *Cyp26a1* is higher than that of *Cyp26c1*. Whereas expression of *Cyp26a1* in the neuroectoderm also begins at E7.5, that of *Cyp26c1* does not begin in the neuroectoderm (r4) until the one-somite stage (Fig. 1A).

Cyp26a1/c1⁻/⁻ mice exhibit severe CNS abnormalities that phenocopy RA embryopathy

To explore whether the apparently normal development of *Cyp26c1⁻/⁻* mice is attributable to functional compensation by *Cyp26a1*, we next generated *Cyp26a1⁻/⁻ Cyp26c1⁻/⁻* (*Cyp26a1/c1⁻/⁻*) mice (Supplementary Fig. 2). In contrast to *Cyp26a1⁻/⁻* or *Cyp26c1⁻/⁻* mice, no viable *Cyp26a1/c1⁻/⁻* embryos were recovered at E11.0 and all double-mutant embryos were absorbed by E12.5 (Supplementary Table 1). At E9.5, *Cyp26a1/c1⁻/⁻* embryos exhibited pronounced CNS abnormalities including a marked reduction in head size, a reduced eye and frontonasal region, and failure of neural tube closure between the forebrain and hindbrain (Fig. 1B). In addition, the first and second branchial arches of the double-mutant embryos appeared hypoplastic. The phenotype of *Cyp26a1/c1⁻/⁻* mice thus appears similar to that of embryos treated with a teratogenic dose of RA (Fig. 1B). Such a phenotype was also observed in a small proportion of *Cyp26a1⁻/⁻* mice (see below). The tailbud, in which only *Cyp26a1* is expressed, showed defects in *Cyp26a1/c1⁻/⁻* embryos similar to those detected in *Cyp26a1⁻/⁻* mice (data not shown) (Sakai et al., 2001). These observations were thus indicative of functional redundancy between *Cyp26a1* and *Cyp26c1*. Given the apparent lack of CNS anomalies in *Cyp26c1⁻/⁻* embryos, they also suggest that CYP26C1 function in the CNS is completely redundant relative to that of CYP26A1, which appears to play the dominant role.

A–P patterning defects in the CNS of Cyp26a1/c1⁻/⁻ mice

To determine the mechanistic basis of the CNS malformations observed in *Cyp26a1/c1⁻/⁻* mice, we first examined the expression of various genes that mark specific segments along the A–P neural axis (Fig. 2A, Supplementary Fig. 4), including *Otx2* (entire forebrain to upper midbrain), *Hoxb1* (r4), *BF1* (ventral telencephalon), *Fgf8* (anterior neural ridge and midbrain–hindbrain junction), *En1* (midbrain to midbrain–hindbrain junction), *Meis2* (midbrain and r2–r3), *Cyp26b1* (predominantly r5 and r6 at E9.5), and *Emx2* (diencephalon). Although most of these markers were expressed in the appropriate A–P order in *Cyp26a1/c1⁻/⁻* embryos at E9.5, the expression domain of *Hoxb1* was markedly expanded anteriorly (Supplementary Fig. 4C). Conversely, the expression domains of *Otx2* and *Meis2* in the midbrain were reduced in size in *Cyp26a1/c1⁻/⁻* embryos (Supplementary Figs. 4C, D), indicative of expansion of the hindbrain at the expense of the forebrain and midbrain.

Molecular patterning defects in the CNS of *Cyp26a1/c1⁻/⁻* embryos were already apparent at E8.5 (Figs. 2A, B). The preotic sulcus and otic sulcus in the hindbrain region were thus absent from *Cyp26a1/c1⁻/⁻* embryos. The expression domain of *Hoxb1* was markedly expanded anteriorly, whereas the level and region of *Otx2* expression were greatly reduced. Consistent with these observations, the expression domain of *Fgf8* was shifted anteriorly and that of *Krox20*, which marks r3 and r5, was observed in a single broad region in the double mutant,

suggesting that the hindbrain was not only expanded but also abnormally patterned. These expression patterns suggest that specification of r1, r2, and r3 is impaired in *Cyp26a1/c1⁻/⁻* embryos. The distribution of the RA signal, as revealed by expression of the *RARE-hsplacZ* transgene, was also extended toward the anterior side in the double-mutant embryos (Figs. 2A, B; Supplementary Fig. 3). The patterning defects of the *Cyp26a1/c1⁻/⁻* CNS were apparent even as early as E7.5 (Supplementary Fig. 5), when *Cyp26a1* and *Cyp26c1* expression begins in the anterior head mesenchyme of WT embryos (Fig. 1A). The boundary between *Otx2* and *Hoxb1* expression domains as well as the anterior border of the *RARE-hsplacZ* expression domain was thus shifted anteriorly in *Cyp26a1/c1⁻/⁻* embryos at E7.5.

Cyp26a1⁻/⁻ mice manifest various defects including tailbud truncation (Abu-Abed et al., 2001; Sakai et al., 2001). However, reexamination of *Cyp26a1⁻/⁻* embryos revealed that some of them showed CNS malformations similar to those of the double mutant. At E9.5, 20% (3/15) of *Cyp26a1⁻/⁻* embryos exhibited an open neural tube resembling that in *Cyp26a1/c1⁻/⁻* embryos, whereas 33% (5/15) and 47% (7/15) of *Cyp26a1⁻/⁻* embryos manifested less pronounced or no obvious CNS defects, respectively (Fig. 1B). At E8.5, the extent of the *Otx2* expression domain was reduced in 29% (2/7) and normal in the remaining 71% (5/7) of *Cyp26a1⁻/⁻* embryos (Fig. 2A). Such phenotypic variation may depend on the level of *Cyp26c1* expression in individual *Cyp26a1⁻/⁻* embryos; indeed, *Cyp26c1* expression was found to be greatly reduced in some *Cyp26a1⁻/⁻* embryos (M.U. et al., unpublished data). Thus, reevaluation of the *Cyp26a1* null mutant revealed incompletely penetrant defects suggestive of an important role for CYP26A1 in regulation of the RA signal during CNS patterning. Together, our results thus indicated that both CYP26A1 and CYP26C1 contribute to CNS patterning and, again, that CYP26A1 plays the dominant role.

An increased level of RA is responsible for the CNS defects of Cyp26a1/c1⁻/⁻ embryos

To determine whether the CNS defects of *Cyp26a1/c1⁻/⁻* embryos are attributable to an increased level of RA, we administered a dose of all-*trans*-RA sufficient to induce malformation of the embryonic CNS (8 mg/kg of body mass) to WT pregnant mice. Administration of RA at both E7.5 and E8.5 induced CNS anomalies in the WT embryos similar to those observed in *Cyp26a1/c1⁻/⁻* embryos, including an open neural tube and underdevelopment of the forebrain and midbrain (Fig. 1B). Furthermore, a single administration of RA at E7.5 induced molecular patterning defects similar to those observed in the *Cyp26a1/c1⁻/⁻* CNS. Expression of *Otx2* was thus reduced, whereas the expression domain of *Hoxb1* was extended toward the anterior end (Fig. 2C). Conversely, we examined whether a lack of RALDH2 would rescue the CNS abnormalities of *Cyp26a1/c1⁻/⁻* embryos. Although *Raldh2⁻/⁻* mice exhibit various defects themselves, especially on the caudal side, the rostral CNS appears relatively normal in these animals (Niederreither et al., 1999) (Fig. 3A). The CNS defects apparent in *Cyp26a1/c1⁻/⁻* embryos were not observed in
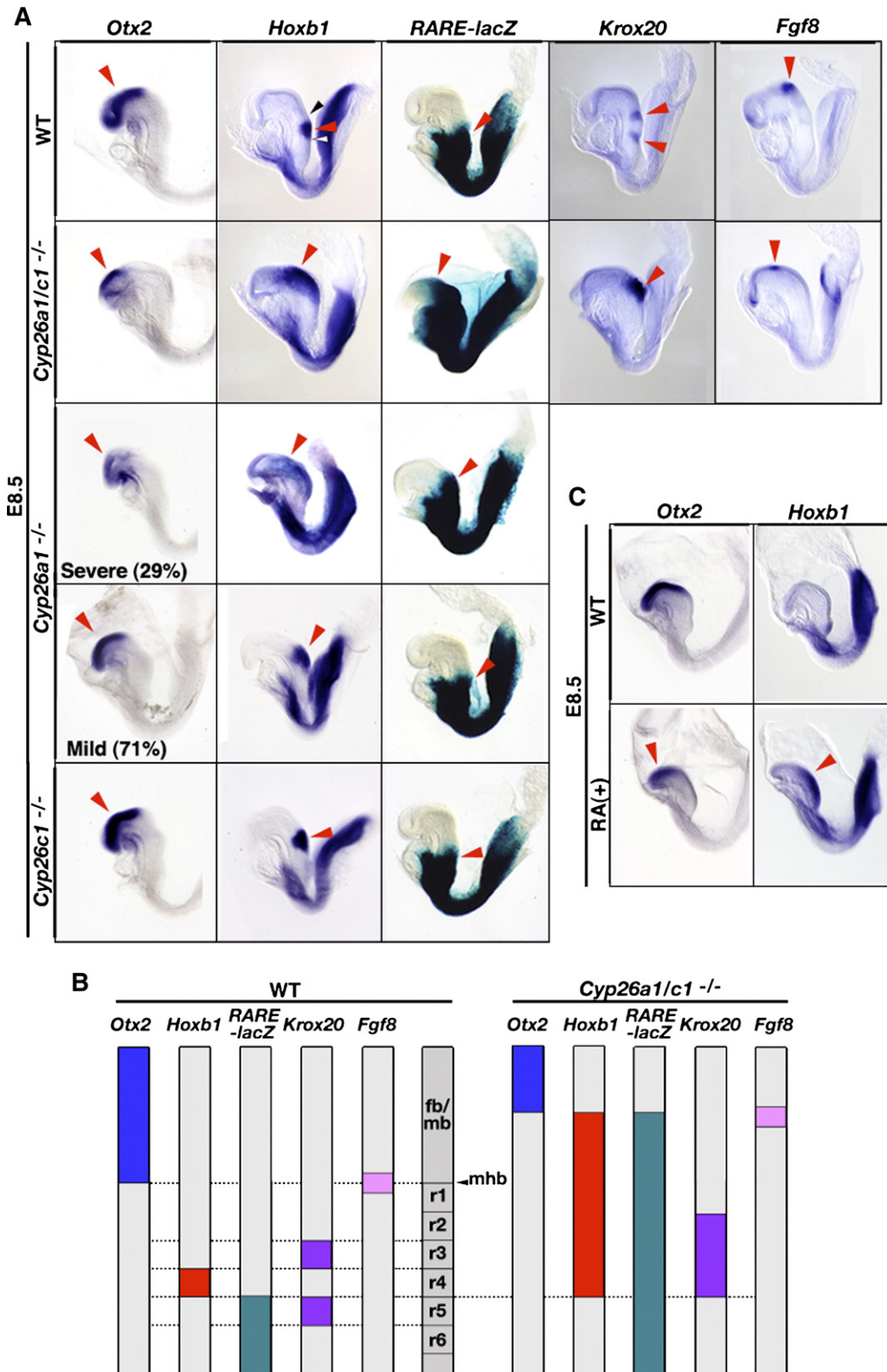
Fig. 2. A–P patterning defects in the CNS of *Cyp26a1/c1*$^{-/-}$ embryos. (A) Expression of *Otx2*, *Hoxb1*, *Krox20*, *Fgf8*, and *RARE-hsplacZ* (red arrowheads) in the CNS of WT, *Cyp26a1/c1*$^{-/-}$, *Cyp26a1*$^{-/-}$, and *Cyp26c1*$^{-/-}$ embryos at E8.5 as revealed by whole-mount in situ hybridization or X-gal staining. The expression domains of *Hoxb1* and *RARE-hsplacZ* were expanded markedly toward the anterior end, whereas that of *Otx2* was greatly reduced, in the double mutant as well as in a minority of *Cyp26a1*$^{-/-}$ embryos. Black and white arrowheads indicate the pre-otic sulcus and otic sulcus, respectively. (B) Schematic representation of the expression domains of the indicated genes in WT and double-mutant embryos at E8.5. fb, forebrain; mb, midbrain; mhb, midbrain–hindbrain boundary; r1 to r6, rhombomeres 1 to 6. (C) Induction by exogenous RA of A–P patterning defects (arrowheads) in the CNS of WT embryos similar to those of *Cyp26a1/c1*$^{-/-}$ embryos. All-*trans*-RA was administered to pregnant WT mice at E7.5; embryos were recovered 24 h later and subjected to whole-mount in situ hybridization.

Cyp26a1/c1$^{-/-}$ Raldh2$^{-/-}$ embryos (Fig. 3A). Furthermore, molecular patterning defects of the *Cyp26a1/c1$^{-/-}$* CNS were rescued by ablation of *Raldh2* (Fig. 3B). These results suggest that an increased level of RA is responsible for malformation of the forebrain and midbrain in *Cyp26a1/c1$^{-/-}$* embryos.

Paucity of head mesenchyme cells in Cyp26a1/c1$^{-/-}$ embryos

Histological analysis revealed that the number of cells in the head mesenchyme was greatly reduced in *Cyp26a1/c1$^{-/-}$*

embryos at E8.75 compared with that in WT embryos (Fig. 3C). This reduction was apparent in the forebrain, midbrain, and anterior portion of the hindbrain but not in the remaining more caudal regions of the CNS (Supplementary Fig. 6). Neither a reduced extent of cell proliferation nor an increased rate of apoptosis appeared to be responsible for the impaired formation of the head mesenchyme in *Cyp26a1/c1$^{-/-}$* embryos, given that immunohistochemical analysis did not reveal abnormal staining either for phosphorylated histone H3 (marker for proliferating cells) or for the active form of
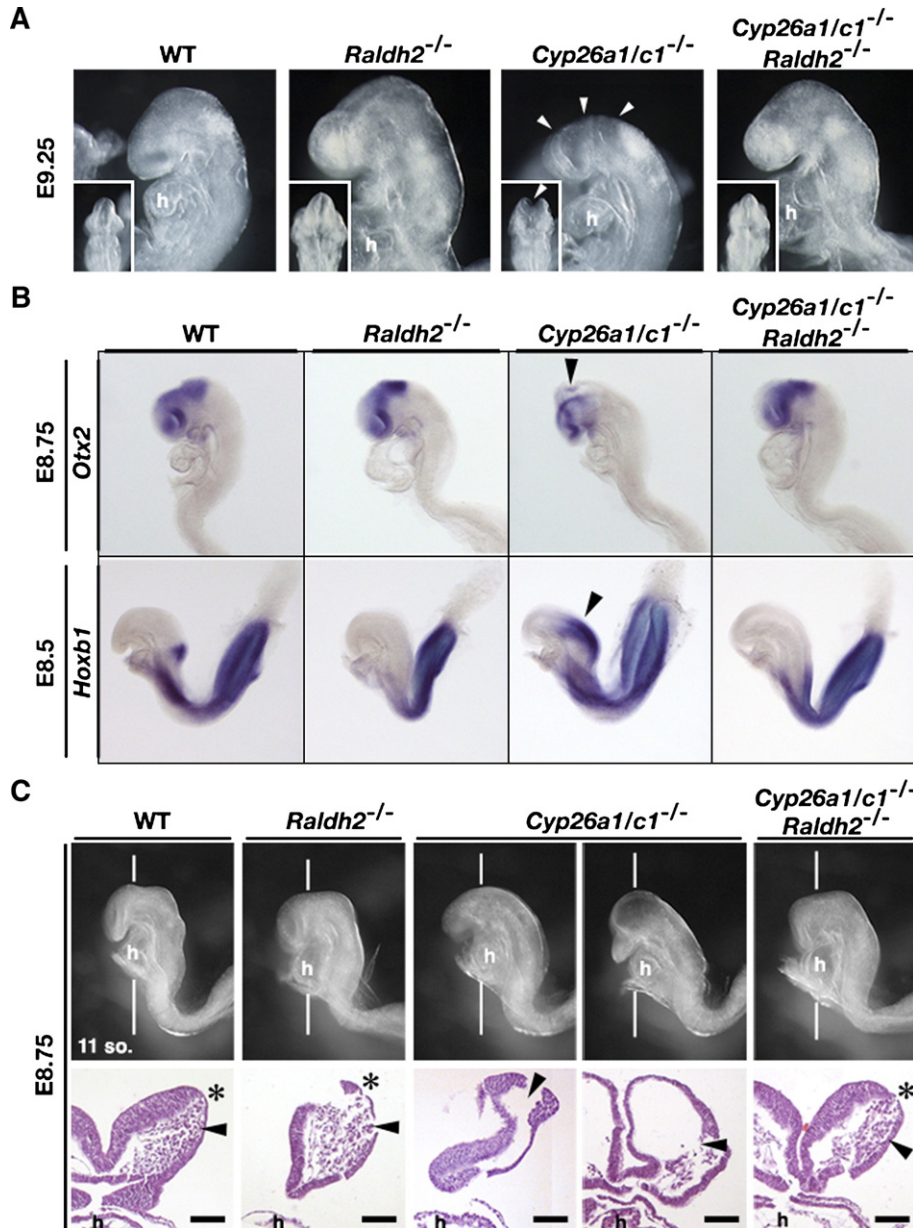

Fig. 3. Rescue of the CNS defects of *Cyp26a1/c1$^{-/-}$* embryos by ablation of *Raldh2*. (A) Lateral (main panels) and dorsal (insets) views of WT, *Raldh2$^{-/-}$*, *Cyp26a1/c1$^{-/-}$*, and *Cyp26a1/c1$^{-/-}$Raldh2$^{-/-}$* embryos at E9.25. The rostral CNS malformations (arrowheads) apparent in *Cyp26a1/c1$^{-/-}$* embryos were not evident in *Cyp26a1/c1$^{-/-}$Raldh2$^{-/-}$* embryos. h, heart. (B) Expression of *Otx2* and *Hoxb1* in the CNS of WT, *Raldh2$^{-/-}$*, *Cyp26a1/c1$^{-/-}$*, and *Cyp26a1/c1$^{-/-}$Raldh2$^{-/-}$* embryos at E8.75 or E8.5. The molecular patterning defects (arrowheads) observed in *Cyp26a1/c1$^{-/-}$* embryos were not apparent in *Cyp26a1/c1$^{-/-}$Raldh2$^{-/-}$* embryos. (C) Hematoxylin–eosin staining of WT, *Raldh2$^{-/-}$*, *Cyp26a1/c1$^{-/-}$*, and *Cyp26a1/c1$^{-/-}$Raldh2$^{-/-}$* embryos at E8.75 (11-somite stage). Two representative *Cyp26a1/c1$^{-/-}$* embryos are shown, one with mild (left) and the other with severe (right) CNS defects. The number of cells in the head mesenchyme (arrowheads) was greatly reduced in *Cyp26a1/c1$^{-/-}$* embryos but was almost normal in *Cyp26a1/c1$^{-/-}$Raldh2$^{-/-}$* embryos. The planes of sections shown in the lower panels are indicated by the horizontal lines through the embryos in the upper panels. Asterisks indicate the regions positive for EMT. Scale bars, 100 μm.

caspase-3 (marker for apoptotic cells) in the forebrain–midbrain regions of the double mutant at a time immediately before that corresponding to the beginning of NCC migration in the WT (Supplementary Fig. 7A). Consistent with these findings, the number of neuroectoderm cells in $Cyp26a1/c1^{-/-}$ embryos at E8.5 was similar to that in the WT (Supplementary Fig. 8).

Head mesenchyme cells originate from both NCCs and mesoderm (Noden, 1988). Mesenchyme cells were detected in the CNS of $Cyp26a1/c1^{-/-}$ embryos at E8.0 (Supplementary Fig. 7B), before the onset of migratory NCC production, suggesting that mesoderm-derived mesenchyme is formed normally and that mesenchyme derived from NCCs is deficient in the double-mutant embryos. Although the production of migratory NCCs was impaired in the entire region between the forebrain and r4 in $Cyp26a1/c1^{-/-}$ embryos at E8.5, a small number of head mesenchyme cells was detected in the presumptive midbrain at E9.25 (Supplementary Fig. 7D) (see below).

Production of migratory cranial NCCs is impaired in $Cyp26a1/c1^{-/-}$ embryos

To confirm further the impairment of migratory cranial NCC production in $Cyp26a1/c1^{-/-}$ embryos, we examined the expression of genes that are expressed specifically in NCCs. In WT embryos at E8.5, NCC-specific markers such as *Snail*, *Sox9*, and *AP2* are expressed in NCCs that emigrate from the forebrain, midbrain, r2, and r4 regions (Fig. 4A, Supplementary Fig. 9); *Sox9* marks premigratory NCCs whereas *Snail* is also expressed in migrating and delaminating NCCs (Figs. 4A, B). Although expression of *Snail*, *Sox9*, and *AP2* was maintained in the neural plate of the forebrain and midbrain regions of $Cyp26a1/c1^{-/-}$ embryos, most of the cells expressing *Snail* remained within the neural plate (Figs. 4A, C). These results suggest that premigratory NCCs are formed normally in $Cyp26a1/c1^{-/-}$ embryos, and that it is the cells derived from NCCs that are lost in the head mesenchyme of the forebrain and midbrain. Intact *Wnt1* expression of the midbrain in double-mutant mice also reinforces this notion (Supplementary Fig. 9).

Given that migratory cranial NCCs are formed by the epithelial–mesenchymal transition (EMT), the loss of head mesenchyme cells in $Cyp26a1/c1^{-/-}$ embryos is likely due to impairment of the EMT of NCCs. The close relation apparent between migratory cranial NCCs and the neuroectoderm–ectoderm junction in WT embryos was not observed in $Cyp26a1/c1^{-/-}$ embryos by histological analysis, which is also suggestive of a severe impairment of the EMT. A similar defect in migratory NCC production, albeit less severe, was observed in RA-treated WT embryos (Fig. 4A). Furthermore, the neuroectoderm–ectoderm junction in $Cyp26a1/c1^{-/-}$ embryos was thickened, suggesting that cranial NCCs that failed to undergo the EMT accumulated in the neural plate. To characterize further the EMT of cranial NCCs, we examined the expression of E-cadherin, which is down-regulated during the EMT in WT embryos (Cano et al., 2000) (Fig. 5A). Expression of E-cadherin was not down-regulated in the region of the
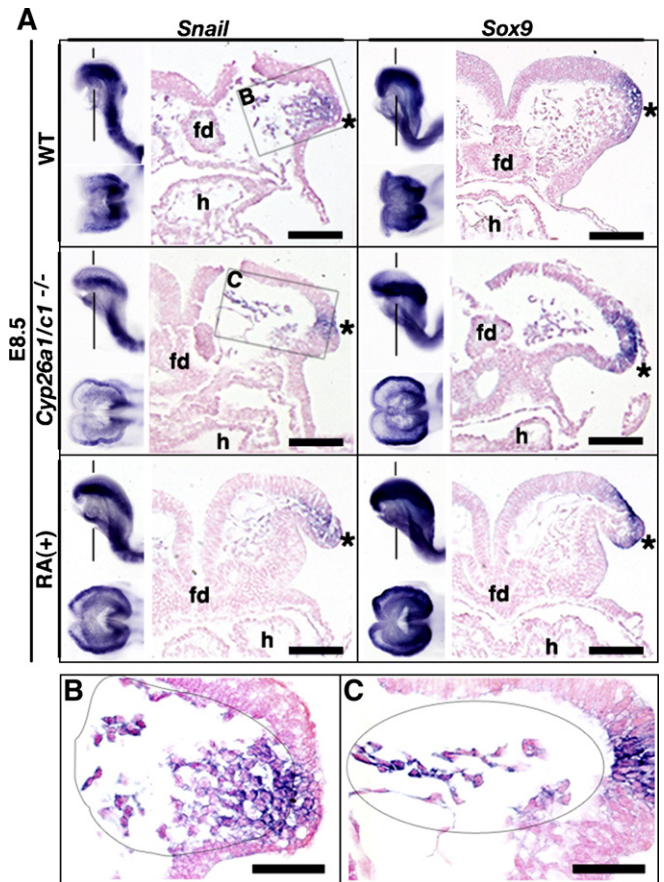

Fig. 4. Intact NCC induction and impaired NCC delamination in $Cyp26a1/c1^{-/-}$ embryos. (A) Expression of *Snail* and *Sox9* in the CNS of WT, $Cyp26a1/c1^{-/-}$, and RA-treated WT embryos at E8.5 (six-somite stage). For each type of embryo, lateral and dorsal views are shown on the left, and frontal sections at the level of the midbrain indicated by the vertical line in the lateral view are shown on the right. In WT embryos, expression of *Snail* and *Sox9* was detected at the edges of the neural plate (asterisks) in premigratory NCCs and that of *Snail* was also apparent in migratory NCCs. In $Cyp26a1/c1^{-/-}$ and RA-treated embryos, however, *Snail* and *Sox9* expression was maintained in the neural plate, but the delamination of NCCs was markedly inhibited (asterisks). The edge of the neural plate was also thickened (asterisks) in $Cyp26a1/c1^{-/-}$ embryos. A close relation between the neuroectoderm and head mesenchyme, representing the delamination of NCCs, was apparent in the WT but not in the double mutant. *Snail*-expressing cells in the head mesenchyme of $Cyp26a1/c1^{-/-}$ embryos were likely derived from the presumptive r4 (see text). fd, foregut diverticulum; h, heart. Scale bars, 100 μm. (B, C) Higher magnification images of the boxed regions in panel A. The outlined areas indicate *Snail*-expressing mesenchyme. Scale bars, 50 μm.

$Cyp26a1/c1^{-/-}$ neural plate in which premigratory NCCs reside (Fig. 5A). Down-regulation of N-cadherin (Nakagawa and Takeichi, 1998) occurred normally in the $Cyp26a1/c1^{-/-}$ embryos (Fig. 5A). The sustained production of E-cadherin in $Cyp26a1/c1^{-/-}$ embryos thus also supports the notion that cranial NCCs fail to undergo the EMT, although N-cadherin is down-regulated normally.

Examination of a series of frontal sections indicated that the production of migratory NCCs was impaired in the entire region between the forebrain and r4, but was normal in more caudal regions, of $Cyp26a1/c1^{-/-}$ embryos (Supplementary Fig. 6). Consistent with this conclusion, the trigeminal (V)
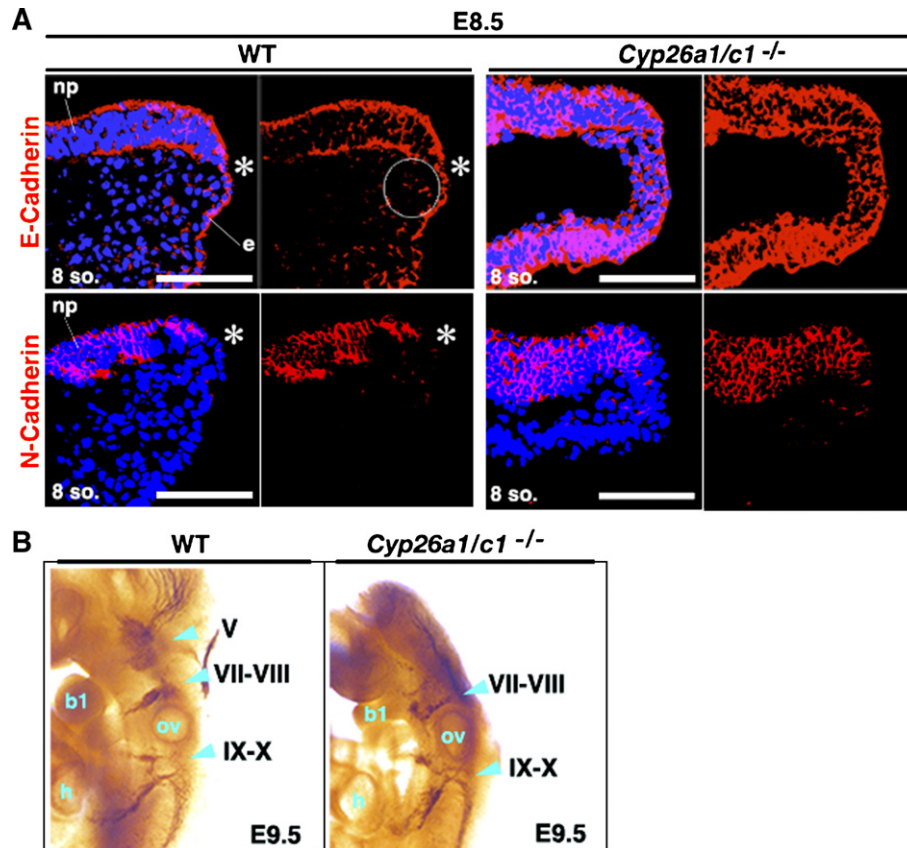
Fig. 5. Cranial NCCs of $Cyp26a1/c1^{-/-}$ embryos fail to undergo the EMT. (A) Immunofluorescence staining for E-cadherin and N-cadherin in frontal sections at the level of the midbrain of WT and $Cyp26a1/c1^{-/-}$ embryos at E8.5 (eight-somite stage). Expression of E-cadherin in the neural plate had undergone down-regulation in the WT embryo but not in the mutant embryo. Expression of N-cadherin in the neural plate did not differ between the two genotypes. Blue fluorescence represents nuclear staining with 4,6-diamidino-2-phenylindole. Asterisks indicate the region positive for EMT, and the circled region contains delaminating NCCs. np, neural plate; e, ectoderm. Scale bars, 100 μm. (B) Cranial ganglia of WT and $Cyp26a1/c1^{-/-}$ embryos at E9.5. Nerves were visualized by neurofilament staining. The trigeminal (V) ganglia, which are derived from NCCs of r2, were missing, r4-derived cranial (VII, VIII) ganglia were hypoplastic, and r6-derived cranial (IX, X) ganglia were normal in $Cyp26a1/c1^{-/-}$ embryos. b1, first branchial arch; ov, otic vesicle; h, heart.

ganglia, which are derived from NCCs of r2, were missing in $Cyp26a1/c1^{-/-}$ embryos (Fig. 5B). The r4-derived cranial (VII, VIII) ganglia were hypoplastic, although the molecular identity of r4 (*Hoxb1*) was not affected, and the r6-derived cranial (IX, X) ganglia were formed normally in the double-mutant embryos. These results suggest that the production of migratory cranial NCCs is inhibited in the region between the forebrain and r4. This conclusion was confirmed by monitoring the fate of the NCC lineage (see below).

We next examined whether a lack of RALDH2 would rescue the failure of migratory NCC production in $Cyp26a1/c1^{-/-}$ embryos. Histological analysis revealed that, in three of six $Cyp26a1/c1^{-/-}Raldh2^{-/-}$ embryos at E8.75, the number of cells in the head mesenchyme was similar to that of WT embryos (Fig. 3C, data not shown), indicating that the migratory NCC production defect of $Cyp26a1/c1^{-/-}$ embryos is indeed rescued by ablation of *Raldh2*. The observed phenotypic variation may depend on the level of maternal RA in individual $Cyp26a1/c1^{-/-}Raldh2^{-/-}$ embryos. An increased level of RA thus appears to be responsible for the defect in migratory cranial NCC production in $Cyp26a1/c1^{-/-}$ embryos.

Fates of cranial premigratory NCCs in Cyp26a1/c1^{−/−} embryos

To examine the fates of premigratory NCCs in $Cyp26a1/c1^{-/-}$ embryos, we labeled these cells in r4 and the midbrain with the fluorescent dye DiI. DiI labeling was performed at the zero- to two-somite stage, before the migration of cranial NCCs begins (Fig. 6A). In WT embryos, the labeled cells in the presumptive r4 region contributed to the second branchial arch whereas those in the presumptive midbrain contributed to the frontonasal region and the first branchial arch (Fig. 6B). These migration patterns are consistent with those observed previously (Osumi-Yamashita et al., 1994). In $Cyp26a1/c1^{-/-}$ embryos, however, NCC migration was markedly impaired. NCCs in the presumptive r4 region migrated toward the second branchial arch but did so more broadly (Fig. 6B). The production of migratory NCCs was thus not completely blocked in the r4 region of the double-mutant embryos. However, the number of migratory NCCs derived from r4 in $Cyp26a1/c1^{-/-}$ embryos was smaller than that apparent in WT embryos, consistent with the observations that the second branchial arch (Fig. 1B) and the facial ganglia (Fig. 5B) are
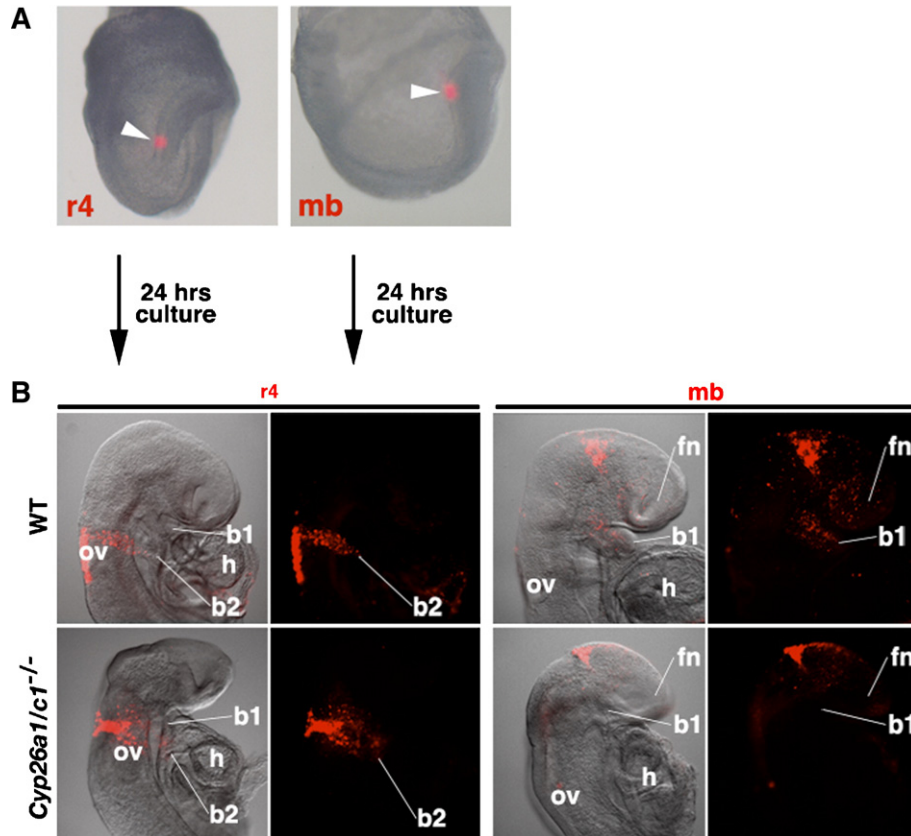
Fig. 6. Fates of cranial premigratory NCCs in *Cyp26a1/c1*$^{-/-}$ embryos. (A) WT embryos injected with DiI (red fluorescence) in the presumptive r4 and midbrain (mb) regions at E8.0. Arrowheads indicate injection sites. (B) WT and *Cyp26a1/c1*$^{-/-}$ embryos injected as in panel A were cultured for 24 h and then examined for the distribution of DiI-labeled cells. Labeled cells that emigrated from the presumptive r4 region were detected in the second branchial arch (b2) of WT embryos but contributed to the anterior region of the mutant embryos. Whereas labeled cells migrated from the presumptive midbrain to the frontonasal (fn) region and the first branchial arch (b1) of WT embryos, they failed to do so in the mutant embryos. Left and right panels in each instance are bright-field and dark-field images, respectively. ov, otic vesicle; h, heart.

hypoplastic in *Cyp26a1/c1*$^{-/-}$ embryos. This small population of detectable migratory NCCs is also consistent with the presence of *Snail*-expressing cells in head mesenchymal tissue of the double mutant at E8.5 (Figs. 4A, C). Similar migration defects were previously observed with RA-treated rat embryos (Lee et al., 1995). Migration of the midbrain NCCs was impaired to an even greater extent in *Cyp26a1/c1*$^{-/-}$ embryos (Fig. 6B). The number of migrating cells was thus greatly reduced, and the labeled cells failed to migrate toward the first branchial arch (or the frontonasal region). Impaired migration of midbrain NCCs is consistent with the observation that the first branchial arch is hypoplastic in *Cyp26a1/c1*$^{-/-}$ embryos (Fig. 1B). However, a small number of cells did migrate anteriorly over a short distance in the mutant embryos (Fig. 6B), possibly explaining the presence of a small number of head mesenchyme cells derived from the midbrain at E9.25 (Supplementary Fig. 7D). Finally, cells positive for the active form of caspase-3 were specifically detected among the premigratory NCCs of *Cyp26a1/c1*$^{-/-}$ embryos at E8.75 (Supplementary Fig. 7C), a stage at which NCC migration has begun in WT embryos, suggesting that NCCs that fail to undergo the EMT are subsequently removed by apoptosis.

Discussion

The role of CYP26C1 in CNS patterning is dependent on cooperation with CYP26A1

It is unknown whether or not the three CYP26 enzymes identified in mammals have identical enzymatic activities in vivo. Biochemical data suggest that the activity of CYP26C1 manifests only slight differences relative to the activities of CYP26A1 and CYP26B1 (Taimi et al., 2004). In spite of such redundancy in activity and the overall similarity in expression patterns between CYP26C1 and CYP26A1, CYP26C1 has been thought to play a role distinct from that of CYP26A1 because of its different expression pattern in the hindbrain (Sirbu et al., 2005). The onset of *Cyp26c1* expression in r4 at E8.0 coincides with the caudal shift of the anterior boundary of the RA signal from r2–r3 to r4–r5, whereas *Cyp26a1* expression is not clearly restricted to pro-rhombomere structures at this stage (Fig. 1A). However, we have now shown that mice that lack CYP26C1 develop without overt abnormalities. The anterior boundary of the RA signal at r4–r5 thus forms correctly and the CNS develops normally in the *Cyp26c1*$^{-/-}$ embryos. In contrast, compared with *Cyp26a1*$^{-/-}$ mice, *Cyp26a1/c1*$^{-/-}$ mice exhibit

additional or more severe defects in regions in which *Cyp26a1* and *Cyp26c1* are coexpressed. These genetic data indicate that CYP26C1 plays a role in CNS patterning in cooperation with CYP26A1. The role of CYP26B1 in determination of the RA signal boundary at r4–r5 remains unclear. The expression of *Cyp26c1* begins at r4 earlier than does that of *Cyp26b1* at r3 and r5 (MacLean et al., 2001; Sirbu et al., 2005), and the *Cyp26b1*$^{-/-}$ mutant does not exhibit a hindbrain patterning defect (Yashiro et al., 2004). Ectopic *Cyp26b1* expression was not detected in *Cyp26c1*$^{-/-}$ embryos (data not shown), but it remains possible that the unchanged boundary of the RA signal at r4–r5 in *Cyp26c1*$^{-/-}$ mice may be due to redundancy not only with CYP26A1 but with CYP26B1.

Regulation of RA distribution along the A–P axis in the CNS

Although exogenous RA exhibits profound pharmacological effects on CNS development (Maden, 2002), the physiological mechanism by which the RA signal synthesized by the embryo itself is controlled appropriately in the CNS has remained unclear. Our data now reveal an essential function of CYP26 enzymes in brain patterning. The correct specification of the forebrain and midbrain requires that the corresponding precursor regions of the developing embryo be maintained devoid of RA through the action of a "CYP26A1-CYP26C1 cassette" in the anterior portion of the CNS. RA thus acts as an anti-anteriorizing factor. It has been suggested that administration of exogenous RA to the chick embryo induces forebrain truncation through down-regulation of *Fgf8* expression in the anterior neural ridge (Creuzet et al., 2004; Schneider et al., 2001). In *Cyp26a1/c1*$^{-/-}$ mice, however, the forebrain is reduced in size but *Fgf8* expression is maintained in the anterior neural ridge. This discrepancy may be due to a difference in the response to RA between chick and mouse embryos. Alternatively, RA synthesized de novo in the body trunk might not diffuse as far as the anterior end of the CNS, given that the most anterior portion of *Cyp26a1/c1*$^{-/-}$ embryos at E7.5 and E8.5 was negative for *RARE-hsplacZ* expression (Fig. 2A, Supplementary Fig. 5). We did not detect ectopic *Cyp26b1* expression in *Cyp26a1/c1*$^{-/-}$ embryos, suggesting that CYP26B1 does not serve as a diffusion barrier in these embryos.

The hindbrain of *Cyp26a1/c1*$^{-/-}$ embryos is also abnormally patterned. Anterior expansion of the *Hoxb1* expression domain up to near the midbrain–hindbrain boundary suggests that r1 to r3 may be misspecified to r4 identity. The lack of *Meis2* expression in this region of *Cyp26a1/c1*$^{-/-}$ embryos is consistent with this notion (Supplementary Fig. 4D). The observations that the trigeminal ganglia were almost completely ablated and that the first branchial arch was severely hypoplastic in *Cyp26a1/c1*$^{-/-}$ embryos are also consistent with this conclusion, although these abnormalities might also be explained by the EMT defect. The analysis of cell lineage with DiI revealed migration of NCCs derived from r4 to inappropriate anterior sites in the double mutant, suggesting that these cells had a mixed-lineage identity of r1 to r4. Such patterning defects in the hindbrain of *Cyp26a1/c1*$^{-/-}$ embryos

are more severe than those previously described for *Cyp26a1*$^{-/-}$ embryos, in which only r3 adopts r4 identity (Sakai et al., 2001).

Cyp26a1 and *Cyp26c1* show dynamic expression in various domains of the mouse embryo (Fig. 1A) (Fujii et al., 1997; Tahayato et al., 2003). The expression of *Cyp26a1* and *Cyp26c1* begins simultaneously at the headfold stage, that of *Cyp26a1* in both the neuroectoderm and head mesenchyme and that of *Cyp26c1* only in head mesenchyme. Previous observations suggested that CYP26A1 first establishes the anterior boundary of the RA signal at r2–r3 and that CYP26C1 in the neuroectoderm (r4) subsequently shifts this boundary to r4–r5 (Sirbu et al., 2005). However, our results now show that this latter boundary was not disrupted in *Cyp26c1*$^{-/-}$ embryos and that most *Cyp26a1*$^{-/-}$ embryos manifest normal hindbrain patterning. We therefore propose a modified model for regulation of the distribution of the RA signal (Fig. 7). First, CYP26A1 and CYP26C1 in the mesenchyme prevent the delivery of RA to the neuroectoderm through head mesenchymal tissue at the headfold stage. The delivery of RA to the rostral CNS region via neuroectoderm is thus restricted. The posterior border of CYP26A1 expression is located more anteriorly in neuroectoderm than in mesenchyme, resulting in a graded distribution of RA in the presumptive hindbrain region that might be responsible for induction of the r2–r3 boundary and r4 identity (Sirbu et al., 2005). The induction of r4 identity through this process may establish *Cyp26c1* expression in r4. It appears that CYP26 initially acts in a non-cell-autonomous manner, given that most *Cyp26a1*$^{-/-}$ embryos show normal or nearly normal CNS development and that the lack of CYP26C1 in the mesenchyme affects the adjacent neuroectoderm in *Cyp26a1/c1*$^{-/-}$ embryos. Given that molecular patterning defects are apparent as early as E7.5 in all *Cyp26a1/c1*$^{-/-}$ embryos, the lack of CYP26 expression not only in the anterior head mesenchyme but also in neuroectoderm at the headfold stage is likely primarily responsible for the impaired A–P patterning of *Cyp26a1/c1*$^{-/-}$ embryos. At the one-somite stage, when *Cyp26c1* is expressed at a high level in r4 of WT embryos, caudal repression of *Hoxb1* expression was apparent in *Cyp26a1/c1*$^{-/-}$ embryos, although the formation of a sharp border at r4–r5 seems slightly disrupted. These results also support the notion that expression of *vHnf1* is sufficient for caudal repression of *Hoxb1* (Sirbu et al., 2005).

RA regulates the production of migratory cranial NCCs

Several lines of evidence suggest that the paucity of head mesenchyme cells in *Cyp26a1/c1*$^{-/-}$ embryos results from an EMT defect of cranial NCCs: (1) The extents of cell proliferation and apoptosis were not affected in *Cyp26a1/c1*$^{-/-}$ embryos at E8.5 (four- to five-somite stage), when NCC delamination has already begun in WT embryos. (2) The histological features of the EMT observed in the midbrain region of WT embryos, including the close relation between head mesenchyme and neuroectoderm, were not apparent in the *Cyp26a1/c1*$^{-/-}$ mutant. (3) NCC induction appeared to be intact in the double mutant, as revealed by the expression patterns of *Wnt1*, *Sox9*, *AP2*, and *Snail* within the neuroectoderm, but the NCCs seemed to
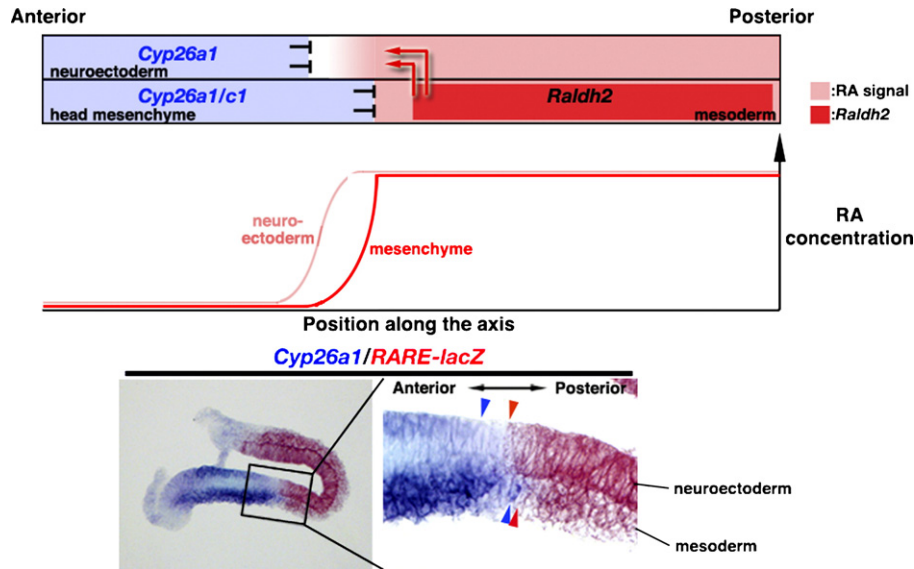
Fig. 7. Model for RA signal regulation along the A–P axis of the early mouse CNS by CYP26 enzymes. The top panel represents the expression domains of *Cyp26a1*, *Cyp26c1*, and *Raldh2* as well as the distribution of the RA signal at E7.5, when *Cyp26b1* expression has not yet begun. Arrows indicate the route of RA delivery. The middle panel shows the putative distribution of RA in neuroectoderm and head mesenchyme (mesoderm). The expression domains of *Cyp26a1* and distribution of the RA signal at E7.5 are shown in the lower panels. A WT embryo harboring the *RARE-hsplacZ* transgene was subjected to Rose-gal staining and then to whole-mount in situ hybridization with a *Cyp26a1* probe at E7.5. Cryosections were then prepared and examined. Blue arrowheads, posterior boundary of *Cyp26a1* expression; red arrowheads, anterior boundary of the RA signal.

remain within the neural plate at the junction between the neuroectoderm and ectoderm. (4) E-cadherin expression was maintained at the junction between the ectoderm and neuroectoderm in *Cyp26a1/c1*$^{-/-}$ embryos. (5) Lineage tracing of NCCs with DiI revealed few migratory cranial NCCs derived from the midbrain region. And (6) E-cadherin induction by RA was previously shown to trigger epithelial differentiation of a breast cancer cell line (Shah et al., 2002). It remains possible that NCCs are lost by apoptosis immediately before the EMT in *Cyp26a1/c1*$^{-/-}$ embryos. However, this is not likely given that apoptotic cells were not detected in these embryos at the four-somite stage, when NCC delamination has already begun in WT embryos. Another possible explanation for the paucity of head mesenchyme cells in the double-mutant embryos is suggested by the observation that many *Cyp26a1/c1*$^{-/-}$ embryos manifested a thin neuroectoderm, indicative of a reduction in total cell number including that of NCC precursors. Whereas the extents of cell proliferation and cell death appeared similar in WT and *Cyp26a1/c1*$^{-/-}$ embryos, it remains possible that some mutant embryos are defective in these processes. Further studies are thus required to assess whether RA inhibits the EMT of cranial NCCs.

Cadherins such as E-cadherin and N-cadherin are down-regulated in delaminated NCCs of WT embryos (Cano et al., 2000; Nakagawa and Takeichi, 1998; Weston et al., 2004; Zhadanov et al., 1999), but E-cadherin was not down-regulated in the region of *Cyp26a1/c1*$^{-/-}$ embryos in which premigratory NCCs reside. This latter finding suggests that the EMT defect in *Cyp26a1/c1*$^{-/-}$ embryos is primarily responsible for the paucity of head mesenchyme, given that down-regulation of cadherins is required for delamination and migration of NCCs (Cano et al., 2000; Nakagawa and

Takeichi, 1998). It has been suggested that Snail mediates down-regulation of expression of the E-cadherin gene (Cano et al., 2000). On the other hand, RA is able to up-regulate E-cadherin expression indirectly (Shah et al., 2002). In *Cyp26a1/c1*$^{-/-}$ embryos, however, E-cadherin failed to undergo down-regulation even in the presence of *Snail* expression, suggesting that down-regulation of E-cadherin is not directly controlled by Snail in vivo, or that E-cadherin expression is regulated by RA and Snail independently. A mechanism for regulation of E-cadherin expression independently of Snail was recently suggested (Zohn et al., 2006). The failure of migratory NCC production was apparent specifically in the region of *Cyp26a1/c1*$^{-/-}$ embryos between the forebrain and r4. In addition, this defect was more severe in more anterior regions. NCCs in the trunk of the mutant embryos gave rise to migratory NCCs normally even though they were exposed to the RA signal. These observations suggest that cranial NCCs, especially those within the midbrain, are sensitive to RA whereas NCCs of the body trunk are resistant to it. Furthermore, the relatively late onset of apoptosis in premigratory NCCs of double-mutant embryos suggests that apoptosis is secondary to failure of migratory cranial NCC production.

How is the defect of migratory cranial NCC production in *Cyp26a1/c1*$^{-/-}$ embryos related to the A–P patterning defects? It is possible that the production defect is directly induced by inappropriate RA signaling as a result of the lack of *CYP26A1* and *CYP26c1* expression beginning at E7.5. The severe production defect was restricted to the forebrain and midbrain, the same regions that showed A–P patterning defects at both morphological and molecular levels, suggestive of a close relation between A–P axis identity and the production of

migratory NCCs. Alternatively, the two types of defects may be independent, given that similar migratory NCC production defects have not been observed in other mouse mutants, such as *Otx2* knockout mice, that exhibit abnormal A–P patterning (Martinez-Barbera et al., 2001). Our results show that, in the presence of the RA signal, cranial NCCs are formed correctly but fail to produce migratory NCCs. Elucidation of the precise mechanism responsible for the failure of migratory cranial NCC production in $Cyp26a1/c1^{-/-}$ embryos may clarify how the delamination of NCCs is regulated.

Acknowledgments

Appendix A. Supplementary data

Supplementary data associated with this article can be found, in the online version, at doi:10.1016/j.ydbio.2006.09.045.

References

Abu-Abed, S., Dolle, P., Metzger, D., Beckett, B., Chambon, P., Petkovich, M., 2001. The retinoic acid-metabolizing enzyme, CYP26A1, is essential for normal hindbrain patterning, vertebral identity, and development of posterior structures. Genes Dev. 15, 226–240.

Avantaggiato, V., Acampora, D., Tuorto, F., Simeone, A., Moroni, M.C., Mavilio, F., Arra, C., Cotelli, F., Nigro, V., 1996. Retinoic acid induces stage-specific repatterning of the rostral central nervous system. Dev. Biol. 175, 347–357.

Cano, A., Perez-Moreno, M.A., Rodrigo, I., Locascio, A., Blanco, M.J., del Barrio, M.G., Portillo, F., Nieto, M.A., 2000. The transcription factor snail controls epithelial–mesenchymal transitions by repressing E-cadherin expression. Nat. Cell Biol. 2, 76–83.

Creuzet, S., Schuler, B., Couly, G., Le Douarin, N.M., 2004. Reciprocal relationships between Fgf8 and neural crest cells in facial and forebrain development. Proc. Natl. Acad. Sci. U. S. A. 101, 4843–4847.

Dupe, V., Lumsden, A., 2001. Hindbrain patterning involves graded responses to retinoic acid signalling. Development 128, 2199–2208.

Fujii, H., Sato, T., Kaneko, S., Gotoh, O., Fujii-Kuriyama, Y., Osawa, K., Kato, S., Hamada, H., 1997. Metabolic inactivation of retinoic acid by a novel P450 differentially expressed in developing mouse embryos. EMBO J. 16, 4163–4173.

Inoue, T., Nakamura, S., Osumi, N., 2000. Fate mapping of the mouse prosencephalic neural plate. Dev. Biol. 219, 373–383.

Koide, T., Downes, M., Chandraratna, R.A., Blumberg, B., Umesono, K., 2001. Active repression of RAR signaling is required for head formation. Genes Dev. 15, 2111–2121.

Lammer, E.J., Chen, D.T., Hoar, R.M., Agnish, N.D., Benke, P.J., Braun, J.T., Curry, C.J., Fernhoff, P.M., Grix Jr., A.W., Lott, I.T., Richard, J.M., Sun, S.C., 1985. Retinoic acid embryopathy. N. Engl. J. Med. 313, 837–841.

Lee, Y.M., Osumi-Yamashita, N., Ninomiya, Y., Moon, C.K., Eriksson, U., Eto,

K., 1995. Retinoic acid stage-dependently alters the migration pattern and identity of hindbrain neural crest cells. Development 121, 825–837.

MacLean, G., Abu-Abed, S., Dolle, P., Tahayato, A., Chambon, P., Petkovich, M., 2001. Cloning of a novel retinoic-acid metabolizing cytochrome P450, Cyp26B1, and comparative expression analysis with Cyp26A1 during early murine development. Mech. Dev. 107, 195–201.

Maden, M., 2002. Retinoid signalling in the development of the central nervous system. Nat. Rev., Neurosci. 3, 843–853.

Maden, M., Gale, E., Kostetskii, I., Zile, M., 1996. Vitamin A-deficient quail embryos have half a hindbrain and other neural defects. Curr. Biol. 6, 417–426.

Martinez-Barbera, J.P., Signore, M., Boyl, P.P., Puelles, E., Acampora, D., Gogoi, R., Schubert, F., Lumsden, A., Simeone, A., 2001. Regionalisation of anterior neuroectoderm and its competence in responding to forebrain and midbrain inducing activities depend on mutual antagonism between OTX2 and GBX2. Development 128, 4789–4800.

Nakagawa, S., Takeichi, M., 1998. Neural crest emigration from the neural tube depends on regulated cadherin expression. Development 125, 2963–2971.

Nebert, D.W., Russell, D.W., 2002. Clinical importance of the cytochromes P450. Lancet 360, 1155–1162.

Niederreither, K., Subbarayan, V., Dolle, P., Chambon, P., 1999. Embryonic retinoic acid synthesis is essential for early mouse post-implantation development. Nat. Genet. 21, 444–448.

Niederreither, K., Vermot, J., Schuhbaur, B., Chambon, P., Dolle, P., 2000. Retinoic acid synthesis and hindbrain patterning in the mouse embryo. Development 127, 75–85.

Noden, D.M., 1988. Interactions and fates of avian craniofacial mesenchyme. Development 103, 121–140.

Nonaka, S., Shiratori, H., Saijoh, Y., Hamada, H., 2002. Determination of left-right patterning of the mouse embryo by artificial nodal flow. Nature 418, 96–99.

Osumi-Yamashita, N., Ninomiya, Y., Doi, H., Eto, K., 1994. The contribution of both forebrain and midbrain crest cells to the mesenchyme in the frontonasal mass of mouse embryos. Dev. Biol. 164, 409–419.

Ray, W.J., Bain, G., Yao, M., Gottlieb, D.I., 1997. CYP26, a novel mammalian cytochrome P450, is induced by retinoic acid and defines a new family. J. Biol. Chem. 272, 18702–18708.

Ross, S.A., McCaffery, P.J., Drager, U.C., De Luca, L.M., 2000. Retinoids in embryonal development. Physiol. Rev. 80, 1021–1054.

Rossant, J., Zirngibl, R., Cado, D., Shago, M., Giguere, V., 1991. Expression of a retinoic acid response element-hsplacZ transgene defines specific domains of transcriptional activity during mouse embryogenesis. Genes Dev. 5, 1333–1344.

Sakai, Y., Meno, C., Fujii, H., Nishino, J., Shiratori, H., Saijoh, Y., Rossant, J., Hamada, H., 2001. The retinoic acid-inactivating enzyme CYP26 is essential for establishing an uneven distribution of retinoic acid along the anterio-posterior axis within the mouse embryo. Genes Dev. 15, 213–225.

Schneider, R.A., Hu, D., Rubenstein, J.L., Maden, M., Helms, J.A., 2001. Local retinoid signaling coordinates forebrain and facial morphogenesis by maintaining FGF8 and SHH. Development 128, 2755–2767.

Shah, S., Pishvaian, M.J., Easwaran, V., Brown, P.H., Byers, S.W., 2002. The role of cadherin, beta-catenin, and AP-1 in retinoid-regulated carcinoma cell differentiation and proliferation. J. Biol. Chem. 277, 25313–25322.

Simeone, A., Avantaggiato, V., Moroni, M.C., Mavilio, F., Arra, C., Cotelli, F., Nigro, V., Acampora, D., 1995. Retinoic acid induces stage-specific antero-posterior transformation of rostral central nervous system. Mech. Dev. 51, 83–98.

Sirbu, I.O., Gresh, L., Barra, J., Duester, G., 2005. Shifting boundaries of retinoic acid activity control hindbrain segmental gene expression. Development 132, 2611–2622.

Tahayato, A., Dolle, P., Petkovich, M., 2003. Cyp26C1 encodes a novel retinoic acid-metabolizing enzyme expressed in the hindbrain, inner ear, first branchial arch and tooth buds during murine development. Gene Expr. Patterns 3, 449–454.

Taimi, M., Helvig, C., Wisniewski, J., Ramshaw, H., White, J., Amad, M., Korczak, B., Petkovich, M., 2004. A novel human cytochrome P450, CYP26C1, involved in metabolism of 9-*cis* and all-*trans* isomers of retinoic acid. J. Biol. Chem. 279, 77–85.

Thompson, J.N., Howell, J.M., Pitt, G.A., McLaughlin, C.I., 1969. The biological activity of retinoic acid in the domestic fowl and the effects of vitamin A deficiency on the chick embryo. Br. J. Nutr. 23, 471–490.

Weston, J.A., Yoshida, H., Robinson, V., Nishikawa, S., Fraser, S.T., 2004. Neural crest and the origin of ectomesenchyme: neural fold heterogeneity suggests an alternative hypothesis. Dev. Dyn. 229, 118–130.

White, J.A., Guo, Y.D., Baetz, K., Beckett-Jones, B., Bonasoro, J., Hsu, K.E., Dilworth, F.J., Jones, G., Petkovich, M., 1996. Identification of the retinoic acid-inducible all-trans-retinoic acid 4-hydroxylase. J. Biol. Chem. 271, 29922–29927.

Wilson, J., Roth, C., Warkany, J., 1953. An analysis of the syndrome of malformations induced by maternal vitamin A deficiency. Effects of restoration of vitamin A at various times during gestation. Am. J. Anat. 92, 189–217.

Yashiro, K., Zhao, X., Uehara, M., Yamashita, K., Nishijima, M., Nishino, J., Saijoh, Y., Sakai, Y., Hamada, H., 2004. Regulation of retinoic acid distribution is required for proximodistal patterning and outgrowth of the developing mouse limb. Dev. Cell 6, 411–422.

Zhadanov, A.B., Provance Jr., D.W., Speer, C.A., Coffin, J.D., Goss, D., Blixt, J.A., Reichert, C.M., Mercer, J.A., 1999. Absence of the tight junctional protein AF-6 disrupts epithelial cell–cell junctions and cell polarity during mouse development. Curr. Biol. 9, 880–888.

Zohn, I.E., Li, Y., Skolnik, E.Y., Anderson, K.V., Han, J., Niswander, L., 2006. p38 and a p38-interacting protein are critical for downregulation of E-cadherin during mouse gastrulation. Cell 125, 957–969.